Spatiotemporal Patterns in Arrays of Coupled Nonlinear Oscillators*

M. Lakshmanan and P. Muruganandam
Centre for Nonlinear Dynamics, Department of Physics
Bharathidasan University, Tiruchirapalli 620 024, India

Abstract

Nonlinear reaction-diffusion systems admit a wide variety of spatiotemporal patterns or structures. In this lecture, we point out that there is certain advantage in studying discrete arrays, namely cellular neural/nonlinear networks (CNNs), over continuous systems. Then, to illustrate these ideas, the dynamics of diffusively coupled one and two dimensional cellular nonlinear networks (CNNs), involving Murali-Lakshmanan-Chua circuit as the basic element, is considered. Propagation failure in the case of uniform diffusion and propagation blocking in the case of defects are pointed out. The mechanism behind these phenomena in terms of loss of stability is explained. Various spatiotemporal patterns arising from diffusion driven instability such as hexagons, rhombous and rolls are considered when external forces are absent. Existence of penta-hepta defects and removal of them due to external forcing is discussed. The transition from hexagonal to roll structure and breathing oscillations in the presence of external forcing is also demonstrated. Further spatiotemporal chaos, synchronization and size instability in the coupled chaotic systems are elucidated.

Contents

*Based on the Dr. Biren Roy Memorial Lecture delivered at Jawaharlal Nehru University by M. Lakshmanan on 27 October 1998

1 Introduction

Patterns abound in nature. If we look around us, we can observe myriads of interesting patterns ranging from uniform to very complex varieties. They occur in varied phenomena encompassing physics, chemistry, biology, social dynamics, economics and so on. Essentially they are distinct structures on a space-time scale, which arise as a collective and cooperative phenomena due to the underlying large number of constituent systems. The latter could be aggregates of particles, atoms, molecules, cells, circuits, defects, dislocations and so on. When these aggregates can move and/or interact, they give rise to the various patterns. A small select set of patterns is shown in Fig. 1. The patterns tell us much about the dynamics of the macroscopic as well as to some extent the microscopic behaviours of the underlying systems. Naturally when the interactions among the constituents are nonlinear, one might expect novel and unexpected patterns.

Patterns could be simple and complex. They could be stationary (eg. still image) or changing with time (eg. recurrent image). They could also tend towards a goal or target asymptotically. Homogeneous or uniform patterns, though trivial, are important basic structures. One can have often travelling wave patterns, especially in *dispersive systems*. Under suitable nonlinear forces, dispersive systems can even admit a different kind of waves namely solitons, which are novel type of localized spatiotemporal patterns, retaining their identity for ever. Perturbations of them can also give rise to further interesting structures. However, even more novel structures which can mimic naturally occurring patterns arise when one considers nonlinear *diffusive* (especially the so called *reaction-diffusion*) *systems*. When large aggregates of microstructures consisting of atoms, molecules, defects, dislocations etc are able to move and interact, the evolution of the concentration of the species can be shown to obey nonlinear diffusive equations of reaction type. They may be deduced from the underlying mass, energy, momentum, etc, balance equations. The general form of the nonlinear reaction-diffusion equation can be given by

$$\frac{\partial c}{\partial t} = \vec{\nabla}.(D\vec{\nabla}c) + f(c, \vec{r}, t). \tag{1}$$

Here c represents the population or concentration density of the species and D and f are, in general, nonlinear functions of c representing the diffusivity and the reaction kinetics, respectively.

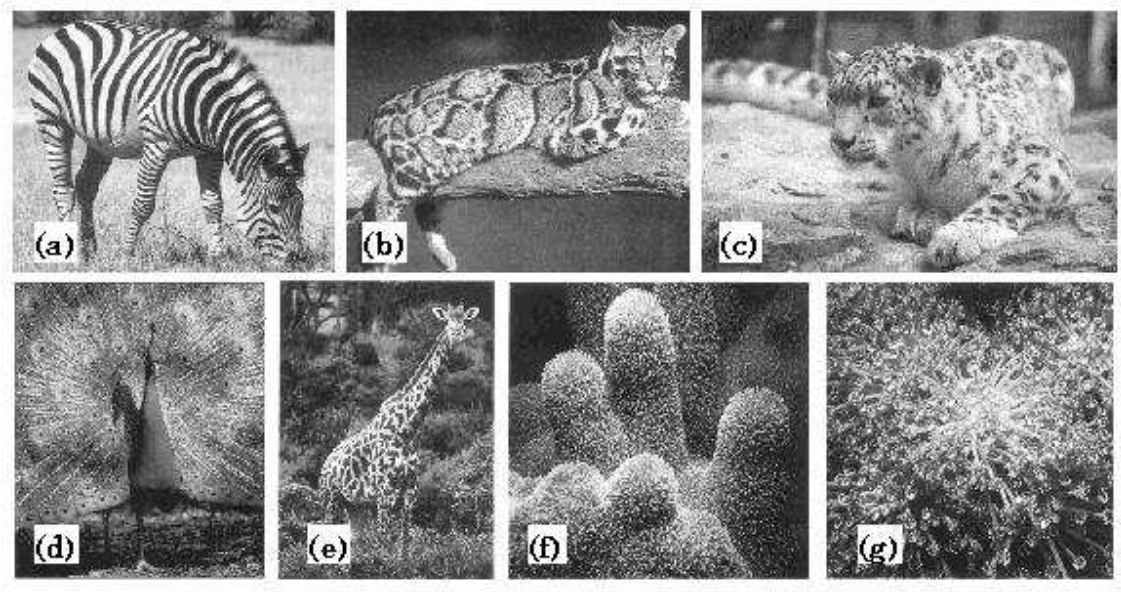

Figure 1: A select band of patterns in natural systems: (a) Zebra (b) Panther (c) snow leopard (d) peacock (e) giraffe (f) pilar coral and (e) daisy coral

For example, one can consider the population density of a particular species and then f in eq. (1) will represent the birth and death processes. In the case of logistic population growth $f = ac(1 - \delta c)$, where a is the linear reproduction rate and δ is the inhibition rate. If D is a constant, then, the above equation (1) will correspond to the celebrated Fisher equation,

$$\frac{\partial c}{\partial t} = D\nabla^2 c + ac(1 - \delta c). \tag{2}$$

Originally Fisher proposed the one dimensional version of the equation in 1937 for the spread of an advantageous gene in a population[1].

1.1 Reaction-diffusion systems

Let us consider the situation in which two or more number of species such as different chemicals, bacteria, populations and so on interact and evolve. In such a situation, one may study the underlying dynamics by considering the appropriate reaction-diffusion equations. Examples include the following systems.

1.1.1 Belousov-Zhabotinsky reaction (Oregonator model)

This is a simple model introduced by Fields, Körös and Noyes of University of Oregon, U.S.A. in 1972 to explain the various features of the Belousov-Zhabotinsky reaction (for details see for example[2]). It can be expressed in a particular form as

$$\begin{aligned} u_{1t} &= D_1\nabla^2 u_1 + \eta^{-1}\left[u_1(1 - u_1) - \frac{bu_2(u_1 - a)}{u_1 + a}\right], \\ u_{2t} &= D_2\nabla^2 u_2 + u_1 - u_2. \end{aligned} \tag{3}$$

Here u_1 represents the concentration of the autocatalytic species $HBrO_2$ and u_2 is the concentration of the transition ion catalyst in the oxidized state Ce^{3+} or Fe^{3+}. η, a and b are parameters. In eq. (3) the suffix t represents partial derivative.

1.1.2 Brusselator model

This is one of the often studied model for the formation of chemical patterns introduced originally by Lefever, Nicolis and Prigogine (see [3]). It is based on the following chemical reaction:

$$\begin{aligned} A &\longrightarrow X, \\ B + X &\longrightarrow Y, \\ 2X + Y &\longrightarrow 3X, \\ X &\longrightarrow E, \end{aligned} \tag{4}$$

where the concentration of the species A, B and E are maintained constant and are thus real control parameters of the system. After appropriate scaling, the evolution of the active species X and Y can be described by the following set of equations[3]:

$$\begin{aligned} \partial_t X &= A - (B+1)X + X^2 Y + D_X \nabla^2 X, \\ \partial_t Y &= BX - X^2 Y + D_Y \nabla^2 Y. \end{aligned} \tag{5}$$

Here D_X and D_Y are diffusion coefficients.

1.1.3 Lotka-Volterra predator-prey model

A model for interacting populations of two species is one in which the population of the prey is dependent on the predator and vice versa. Such systems can be represented by the following set of equations[4]:

$$\begin{aligned} \frac{\partial S_1}{\partial t} &= D_1 \frac{\partial^2 S_1}{\partial x^2} + a_1 S_1 - b_1 S_1 S_2, \\ \frac{\partial S_2}{\partial t} &= D_2 \frac{\partial^2 S_2}{\partial x^2} - a_2 S_2 + b_2 S_1 S_2. \end{aligned} \tag{6}$$

Here S_1 and S_2 are the population densities of prey and predator, D_1 and D_2 are the diffusivities of the two populations, respectively. a_1, a_2 are the linear ratio of birth and death for the individual species; b_1 and b_2 are the linear decay and growth factors due to interaction.

1.1.4 Gierer-Meinhardt model for biological pattern formation

The possible interaction of an activator and a rapidly diffusing inhibitor can be modeled by the following set of equations[5]:

$$\begin{aligned} \frac{\partial a}{\partial t} &= D_a \Delta a + \rho_a \frac{a^2}{1 + \kappa_a a^2} - \mu_a a + \sigma_a, \\ \frac{\partial h}{\partial t} &= D_h \Delta h + \rho_h a^2 - \mu_h h + \sigma_h. \end{aligned} \tag{7}$$

Here μ_a, μ_h are removal rates, ρ_a, ρ_h are the cross reaction coefficients and σ_a, σ_h are the basic products of the activator and inhibitor, respectively. κ_a corresponds to the saturation constant.

1.1.5 FitzHugh-Nagumo nerve conduction model

A well known model for impulse propagation along the neuronal axons of living organisms is the FitzHugh-Nagumo model represented by the following set of equations[6],

$$\begin{aligned} V_t &= V_{xx} + V - \frac{V^3}{3} - R + I(x,t), \\ R_t &= c(V + a - bR). \end{aligned} \tag{8}$$

Here V represents the action potential and R corresponds to the lumped refractory variable. $I(x,t)$ is the external injected current, a, b are positive constants and c corresponds to the temperature factor.

2 Spatiotemporal patterns in reaction-diffusion systems

In the above, we have mentioned a few reaction-diffusion systems that arise under different physical, chemical and biological contexts. Next it is of considerable interest to look into the distinct space-time structures or spatiotemporal patterns which are admitted by these systems. Specifically we may mention the following structures:

- uniform or homogeneous steady states (trivial)
- autowaves including travelling waves
- spiral waves
- Turing patterns (rolls, stripes, hexagons, rhombs, etc.)
- localized structures
- spatiotemporal chaos

and so on. Among these patterns some of them (eg. Turing patterns) may also be identified as *dissipative structures* as they emerge spontaneously from homogeneous equilibrium states and correspond to systems driven away from thermodynamic equilibrium. In the following we will briefly discuss the various space-time structures.

2.1 Homogeneous patterns

The trivial, but important, class of patterns is the homogeneous or uniform steady states. These are the equilibrium solutions of the governing equations. Interesting dynamical features such as the formation of various nonhomogeneous spatiotemporal patterns will arise when these homogeneous states lose their stability.

2.2 Autowaves

Transport processes in physical, chemical and physiological systems have been often associated with special types of waves, namely travelling waves. In general, these types of waves are termed as *autowaves* or *autonomous waves*[7]. These autowaves can propagate in an active excitable medium at the expense of energy stored in the medium even in the absence of external driving forces. One has to note that dispersive systems often admit different kinds of propagating waves, called classical waves, such as sinusoidal travelling waves, wave packets, solitary waves, solitons and so on. However, all these dispersive waves carry energy and information and do not consume any energy associated with the medium. The medium in these cases is said to be passive. On the other hand, autowaves propagate in nonlinear diffusive as well as dissipative systems in a self sustained manner by inducing a local release of the stored energy and use it to trigger the same process in the adjacent regions. The medium here is termed as active medium. Typical examples include the waves of combustion (eg. flame propagating along the cord of a cracker), waves of phase transition, concentration waves in chemical reactions, nerve impulse propagation in neuronal axons, excitation waves in cardiac tissues, epidemic waves in ecological populations and so on.

Few important classes of autowaves which arise in many physical, chemical and biological reaction-diffusion systems are the travelling wavefronts, travelling pulses, travelling wave trains and so on. An example for the travelling wavefront is the solution of the Fisher equation (2), in one spatial dimension, of the form

$$u = u(x - ct) \equiv u(\zeta), \quad \zeta = x - ct.$$

Here c is the wave speed. Travelling pulses arise for example in the FitzHugh-Nagumo nerve conduction model (8). Typical example for the travelling wavetrain is the wave solution of λ - ω systems[8].

2.3 Spiral waves

Another interesting class of waves which are very common in a variety of natural systems corresponds to the *spiral waves* and *scroll waves* that arise in more than one spatial dimensions. The spiral waves which arise in two spatial dimensions can be realized by considering a single wave propagating around a circular obstacle[9]. The wave repeatedly travels along the same path at a frequency given by the wave velocity divided by the circumference of the obstacle. If the radius is gradually decreased the frequency of the obstacle increases until the wavefront of a new wave catches up with the tail of the previous wave. At this point the rate at which the wave travels around the obstacle cannot increase further because the new wave cannot re-excite regions that are still recovering from the previous wave.

If the radius is made even smaller, the wave is forced to adopt a spiral shape that continues to rotate around a central core (see Fig. 2(c)). The spiral cannot enter the central core because this region is still in the so called refractory (or recovering) state and cannot be re-excited. An

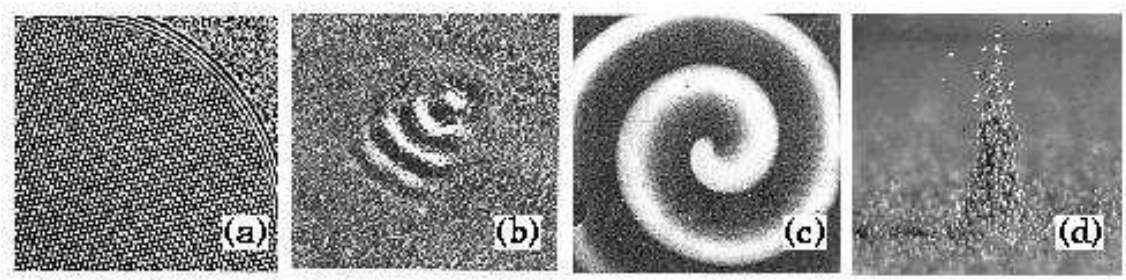

Figure 2: (a) Hexagonal pattern in Rayleigh-Bénard system (b) Localized propagating wave in binary fluid convection (c) Sprial wave in the Belousov-Zhabotinsky reaction and (d) Localized standing wave in vertically vibrated layer of bronze balls

example for the spiral wave is the case of cardiac arrhythmia in the heart during an irregularity in the heartbeat. The phenomenon is known to be modeled by Hodgkin-Huxley model. Another example is the spiral patterns in the Belousov-Zhabotinsky (BZ) reaction where scroll waves have also been observed. Recent studies show the generation of scroll waves in photosensitive excitable media by perturbing travelling waves to their direction of propagation[10]

2.4 Turing patterns

Yet another important kind of patterns which arises in reaction-diffusion systems is the Turing pattern. A. M. Turing in 1952 suggested that, under certain conditions, chemicals can react and diffuse in such a way to produce steady state heterogeneous patterns of chemicals[11]. He had also proposed a model for the chemical basis of *morphogenesis* (which represents the development of structure during the growth of an organism). Turing patterns arise in many reaction-diffusion systems when a homogeneous steady state which is stable due to small spatial perturbations in the absence of diffusion becomes unstable in the presence of diffusion combined with the condition that one of the species or chemicals should diffuse faster than the other. Typical examples include, hexagonal patterns in Rayleigh-Bénard system, the formation of spots in leopard, stripes in zebra, fingerprint patterns and so on. In order to understand the formation of Turing patterns, let us consider the model for the two chemical species represented by the following set of rescaled reaction-diffusion equations:

$$\begin{aligned} \frac{\partial u}{\partial t} &= \gamma f(u,v) + \nabla^2 u, \\ \frac{\partial v}{\partial t} &= \gamma g(u,v) + d\nabla^2 v. \end{aligned} \tag{9}$$

Here u and v are the rescaled concentration of the two chemical species, f and g are, in general, nonlinear functions of u and v representing the kinetics. Suppose (u_0, v_0) is the homogeneous steady state, which is stable when the diffusion is absent and becomes unstable in the presence of diffusion. Then one can write the condition for the diffusion driven instability as[8]

$$\begin{aligned} f_u + g_v &< 0, \\ f_u g_v - f_v g_u &> 0, \\ d f_u + g_v &> 0, \\ (d f_u + g_v)^2 - 4d(f_u g_v - f_v g_u) &> 0, \end{aligned} \tag{10}$$

where f_u, f_v, g_u and g_v are the derivatives of the functions f and g evaluated at the steady state (u_0, v_0). These conditions can be further used for a selection of the admissible wavenumbers associated with the instability, leading to spontaneous formation of nontrivial spatial patterns.

2.5 Localized structure

Recently it has been found that certain dissipative nonlinear systems when driven by external forces exhibit a novel class of localized structures. Such structures have been observed in several experimental and theoretical models[12, 13, 14]. For example, vertically vibrarted granuler layer shows a kind of localized oscillations called *oscillons*. These oscillons are highly localized particle-like excitations (see Fig. 2(d)) of the granular layer which oscillate at half the driving frequency. Other examples includes localized oscillations in fluid systems[13], breathing solutions of Ginzburg-Landau equations[14] and so on. Essentially these localized structures arise due to a tendency of certain nonlinear sytems which localize dissipation in the presence of external forces.

2.6 Spatiotemporal chaos

The study of spatiotemporal or extensive chaos has also been receiving considerable interest in recent times. The phenomenon of chaos in low dimensional systems is almost well understood. However there is a lot to be investigated in extended systems. Studies on extended systems show that the fractal dimension increases linearly with the system size. Further there are measures such as multiple positive Lyapunov exponents, spatial correlation length, information functions and so on to quantify the spatiotemporal chaos[15, 16].

3 Cellular neural/nonlinear networks (CNNs) as reaction-diffusion systems

The most common factor in the autowave process and other pattern formations in reaction-diffusion systems is the presence of active nonlinear medium. We have already discussed the role of active medium in the previous subsection for the autowave process. However there are physical situations where propagation of waves is inhibited beyond certain spatial distances in such medium, for example, the failure of electrical impulse in the nerves of patients suffering from *multiple sclerosis*. Unfortunately there are theorems[17] which clearly shows that continuous models cannot exhibit such *propagation failure*. In order to simulate this kind of new phenomenon, in addition to the existing several kinds of patterns noted above, it becomes necessary to consider discrete versions of diffusively coupled nonlinear dynamical systems to mimic reaction-diffusion processes. In many situations, the discrete systems are modeled by appropriate nonlinear electronic circuits, for example the cases of impulse propagation along nerve fiber, propagation of action potential in cardiac tissues and so on.

Under these circumstances, it is of great interest to investigate the dynamics of arrays of diffusively coupled nonlinear oscillators and systems. In such cases one can often consider an array of interconnected locally coupled cells such as neurons, nonlinear circuits, nonlinear oscillators and

so on. Such aggregates of cells may be called *cellular neural networks* (CNNs) in the case of neurons and *cellular nonlinear networks* (again CNNs) in the case of oscillators and circuits[18, 19].

3.1 Cellular Neural Networks (CNNs)

In general, a CNN is defined mathematically[19] by the dynamics of the constituent subsystems (state equations of the individual oscillators or cells) and a *synaptic law* which specifies the interaction with their neighbours. Such cellular neural networks, namely, interconnections of sufficiently large number of simple dynamical units can exhibit extremely complex, synergetic and self organizing behaviours. Theoretically one can consider a system of coupled ordinary differential equations (odes) to represent a macroscopic system, in which each of the odes corresponds to the evolution of the individual subsystem. Such collection or aggregates could represent the *discrete reaction-diffusion systems*[20]. In other words, in reaction-diffusion systems, the CNNs have linear synaptic law which approximates the spatial Laplacian operator (nearest neighbour coupling). A CNN can be represented by the following four specifications[19]:

1. The cell dynamics given by

$$\dot{x}_j = g_j(x_j) + I_j(x_1, x_2 \ldots x_{j-1}, x_j, x_{j+1} \ldots x_m), \quad j = 1, 2 \ldots m,$$

   where I_j represents to the interaction between the j^{th} and the remaining cells.

2. A synaptic law representing the interaction between the cells. For the reaction-diffusion CNN this can be given by the discrete spatial Laplacion operator.

3. Appropriate boundary conditions.

4. Initial conditions.

Specific examples are the coupled array of anharmonic oscillators[21], Josephson junctions[22], continuously stirred tank reactors (CSTR) exhibiting travelling waves[23, 24], propagation of nerve impulses (action potential) along the neuronal axon[6], the propagation of cardiac action potential in the cardiac tissues[25] and so on. For the past few years several investigations have been carried out to understand the spatiotemporal behaviours of these coupled nonlinear oscillators and systems. The studies on these systems include the travelling wave phenomena, Turing patterns, spatiotemporal chaos and synchronization[26, 27, 28, 29, 30, 31, 32]. Of particular interest among coupled arrays is the study of *diffusively coupled driven systems* as they represent diverse topics like Faraday instability[33], granular hydrodynamics[12, 34], self organized criticality[35] and so on. Identification of localized structures in these systems has been receiving considerable attention very recently[13].

A rather powerful and practical way of studying CNN systems is to model the constituent cells in terms of suitable nonlinear electronic circuits, which are then interconnected through appropriate linear resistors. The advantages of such arrays of nonlinear electronic circuits is that they are quite flexible, that is they can mimic real systems but also can be studied on their own merit, they are easy to produce and easy to study experimentally and numerically. From this point of view already Pérez-Muñuzuri et al have studied the dynamics of CNNs with the three variable Chua's circuit as the basic element and identified several interesting patterns. However it will be considerable interest if one investigates the dynamics of very simple diffusively coupled driven nonlinear electronic circuits to realize novel spatiotemporal patterns. Recently Murali, Lakshmanan and Chua[48] have introduced the simplest second order nolinear nonautonomous disspative circuit consisting of a single nonlinear element, namely, the Chua's diode. This simple circuit can exhibit a variety of interesting bifurcations, chaos and so on when driven by external periodic force[36, 37, 38]. Therefore it will be of considerable interest to steady the dynamics of one and two dimensional arrays of coupled MLC circuts. In this lecture, we wish to give brief details of the type of spatiotemporal patterns and other features which arise in arrays of coupled MLC circuits with and without the presence of external force.

3.2 Murali-Lakshmanan-Chua circuit

The Murali-Lakshmanan-Chua circuit, Fig. 3(a), is the simplest second order dissipative non-autonomous circuit, consisting of Chua's diode as the only nonlinear element[36]. This circuit contains a capacitor (C), an inductor (L), a linear resistor (R), an external periodic forcing ($f \sin \Omega t$) and a Chua's diode. By applying the Kirchoff's laws to this circuit, the governing

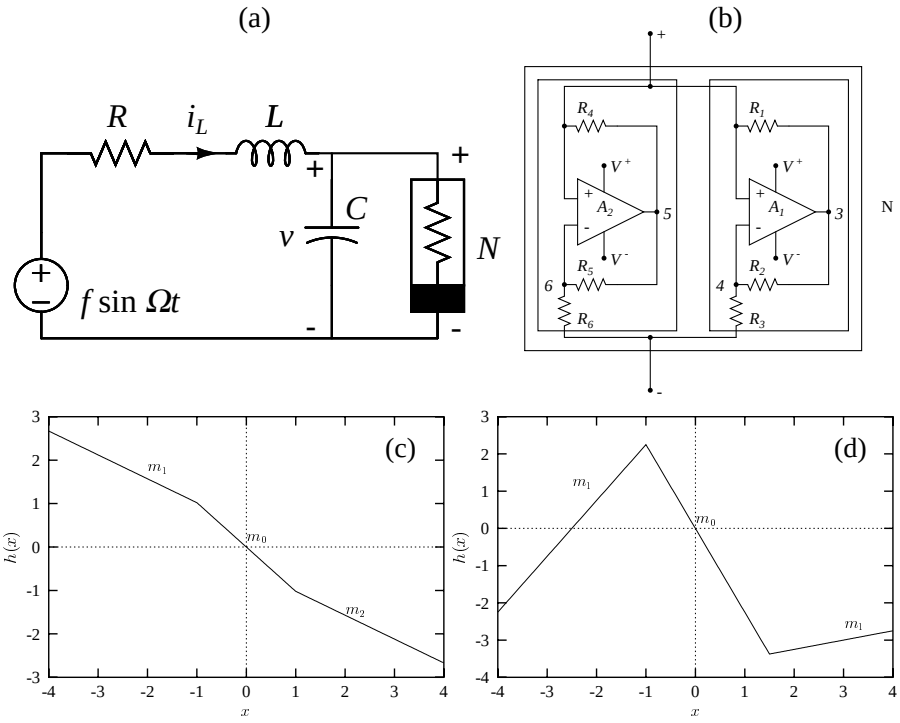

Figure 3: (a) Circuit realization of the simple MLC circuit (b) Circuit realization of the Chua's diode. The characteristic curve for the Chua's diode ($h(x)$) for (c) $\{m_0, m_1, m_2\} = \{-1.02, -.55, -0.55\}$ and (d) $\{m_0, m_1, m_2\} = \{-2.5, 1.5, 0.25\}$

equations for the voltage v across the capacitor C and the current i_L through the inductor L are represented by the following set of two first order nonautonomous differential equations:

$$\begin{aligned} C\frac{dv}{dt} &= i_L - g(v), \\ L\frac{di_L}{dt} &= -Ri_L - R_s i_L - v + f \sin \Omega t, \end{aligned} \tag{11}$$

where $g(v)$ is a piecewise linear function corresponding to the characteristic of the Chua's diode (N) and is given by

$$g(v) = \begin{cases} \epsilon' + G_2 v + (G_0 - G_1), & v > B_p \\ \epsilon' + G_0 v, & -B_p \le v \le B_p \\ \epsilon' + G_1 v - (G_0 - G_1), & v < -B_p \end{cases} \tag{12}$$

The piecewise nature of the characteristic curve of Chua's diode is obvious from Eq. (12). The slopes of left, middle and right segments of the characteristic curve are G_1, G_0 and G_2, respectively. $-B_p$ and B_p are the break points and ϵ' corresponds to the dc offset in the Chua's diode. Rescaling Eq. (11) as $v = xB_p$, $i_L = GyB_p$, $G = 1/R$, $\omega = \Omega C/G$, $t = \tau C/G$ and $\epsilon = \epsilon'/G$

and then redefining τ as t the following set of normalized equations are obtained:

$$\begin{aligned} \dot{x} &= y - h(x), \\ \dot{y} &= -\beta x - \sigma y + F \sin \omega t, \end{aligned} \tag{13}$$

with

$$h(x) = \begin{cases} \epsilon + m_2 x + (m_0 - m_1), & x \geq x_2 \\ \epsilon + m_0 x, & x_1 \leq x \leq x_2 \\ \epsilon + m_1 x - (m_0 - m_1), & x \leq x_1 \end{cases}, \tag{14}$$

where $\beta = (C/LG^2)$, $\sigma = (C/LG^2)(1+GR_s)$ and $F = (f\beta/B_p)$. Obviously $h(x)$ takes the form as in Eq. (14) with $m_0 = G_0/G$, $m_1 = G_1/G$ and $m_2 = G_2/G$. The dynamics of Eq. (13) depends on the parameters β, σ, m_0, m_1, m_2, ϵ, ω and F.

The rescaled parameters in the experimental observations correspond to $\beta = 1.0$, $\sigma = 1.015$, $m_0 = -1.02$, $m_1 = -0.55$, $m_2 - 0.55$, $\epsilon = 0$ and $\omega = 0.75$. By varying F one can observe the familiar period doubling bifurcations leading to chaos and several periodic windows in the MLC

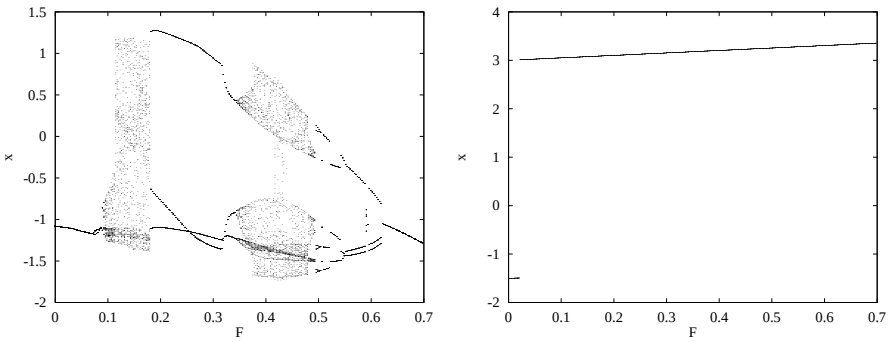

Figure 4: Bifurcation diagram in the $F - x$ plane (a) for $\{m_0, m_1, m_2, \epsilon, \beta, \sigma, \omega\} = \{-1.02, -.055, -0.55, 0.0, 1.0, 1.015, 0.75\}$ and (b) for $\{m_0, m_1, m_2, \epsilon, \beta, \sigma, \omega\} = \{-2.25, 1.5, 0.25, 0.0, 1.0, 1.0, 0.75\}$

circuit. Fig. 4(a) shows the one parameter bifurcation diagram in the $F-x$ plane [$F \in (0, 0.7)$]. A summary of bifurcations that occur in this case for different F values is given in Table 1. Further it is of great interest to consider the parametric choice $\{m_0, m_1, m_2, \epsilon, \beta, \sigma, \omega\} = \{-2.25, 1.5, 0.25, 0.0, 1.0, 1.0, 0.75\}$ which corresponds to the function $h(x)$ having the form as shown in Fig. 3(d). This choice of parameters provides the possibility of bistability nature in the asymmetric case in the absence of periodic forcing. In this case one can easily observe from numerical simulations that the MLC circuit admits only limit cycles for $F \in (0, 0.7)$. The bifurcation diagram in the $F - x$ plane is depicted in Fig. 4(b).

Table 1: Summary of bifurcation phenomena of Eq. (13)

amplitude (F)	description of attractor
$0 < F \leq 0.071$	period-1 limit cycle
$0.071 < F \leq 0.089$	period-2 limit cycle
$0.089 < F \leq 0.093$	period-4 limit cycle
$0.093 < F \leq 0.19$	chaos
$0.19 < F \leq 0.3425$	period-3 window
$0.3425 < F \leq 0.499$	chaos
$0.499 < F \leq 0.625$	period-3 window
$0.625 < F$	period-1 boundary

3.3 Present study

In the following we discuss the active wave propagation and various spatiotemporal patterns associated with the one and two dimensional CNNs represented by diffusively coupled MLC circuits. First we made a critical review on the active wave propagation that occurs in the autonomous system by analysing the linear stability properties of the coupled systems. This analysis give us a clear understanding of the wave propagation in coupled systems which is essentially the loss of stability of the steady states via subcritical bifurcation coupled with the existence of necessary basin of attraction for the steady states associated with the coupled system. We also discuss the effect of weak coupling on the active wave propagation which causes a blocking of the wave when it reaches the weakly coupled cell. Then we look into various spatiotemporal patterns due to the presence of Turing instabilty in the absence of external force.

Further as mentioned earlier it is of great physical interest to study the dynamics of the coupled oscillators when individual oscillators are driven by external forces. We study the spatiotemporal patterns in the presence of periodic external force and investigate the effect of it on the propagation phenomenon and Turing patterns. Depending upon the choice of control parameters, a transition from hexagons to regular rhombic structures, hexagons to rolls and then to breathing oscillations from hexagons are observed. The presence of external force with sufficient strength removes the penta-hepta defect pair originally present in the spontaneously formed hexagonal patterns leading to the formation of regular rhombic structures. The inclusion of external periodic force can also induce a transition from hexagons to rolls provided there are domains of small roll structures in the absence of force. We further show that in the region of Hopf-Turing instability, the inclusion of external periodic force with sufficiently small amplitude induces a type of breathing oscillations though the system shows a regular hexagonal pattern in the absence of any external force.

Finally, we also study the spatiotemporal chaotic dynamics of the one dimensional array of MLC circuits when individual oscillators oscillate chaotically. In this case, the emergence of spatiotemporal patterns depends on the system size. For larger size, above a critical number of cells, we observe a controlled space-time regular pattern eventhough the single MLC circuit itself oscillates chaotically. However, synchronization occurs for a smaller system size, below the threshold limit.

4 Arrays of Murali-Lakshmanan-Chua (MLC) circuits

As mentioned in the introduction (see 3.2), the circuit proposed by Murali, Lakshmanan and Chua (MLC) is one of the simplest second order dissipative nonautonomous circuit having a single nonlinear element[36]. Here we will consider one and two dimensional arrays of such MLC circuits, where the intercell couplings are effected by linear resistors.

4.1 One-dimensional array

Fig. 5 shows a schematic representation of an one dimensional chain of resistively coupled MLC circuits. The dynamics of the one dimensional chain can be easily shown to be governed by the following system of equations, in terms of suitable rescaled variables,

$$\dot{x}_i = y_i - h(x_i) + D(x_{i+1} + x_{i-1} - 2x_i), \tag{15}$$

$$\dot{y}_i = -\sigma y_i - \beta x_i + F \sin \omega t, \quad i = 1, 2, \cdots, N, \tag{16}$$

where D is the diffusion coefficient, N is the chain length and $h(x)$ is a three segment piecewise linear function representing the current voltage characteristic of the Chua's diode and given in eq. (14). In (14) m_0, m_1 and m_2 are the three slopes. Depending on the choice of m_0, m_1 and m_2 one can fix the characteristic curve of the Chua's diode. Here ϵ corresponds to the dc offset. In our analysis, we will consider a few typical forms of $h(x)$ for which the coupld MLC circuits exhibit interesting dynamics such as active wave propagation, Turing patterns, spatiotemporal chaos and so on. In the following studies we will consider a chain of $N = 100$ MLC circuits.

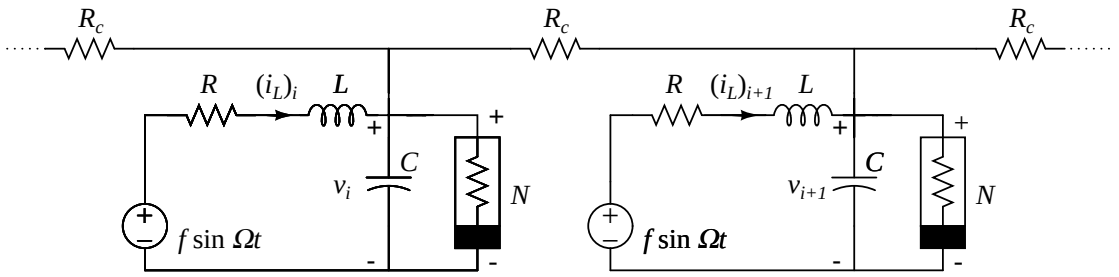

Figure 5: Circuit diagram showing one dimesnional array of coupled MLC circuits

4.2 Two-dimensional array

As in the case of the one dimensional array introduced above, one can also consider a two dimensional array with each cell in the array being coupled to four of its nearest neighbours with linear resistors. The model equation can be now written in dimensionless form as

$$\begin{aligned} \dot{x}_{i,j} &= y_{i,j} - h(x_{i,j}) + D_1(x_{i+1,j} + x_{i-1,j} + x_{i,j+1} + x_{i,j-1} - 4x_{i,j}) \\ &\equiv f(x_{i,j}, y_{i,j}), \qquad (17) \\ \dot{y}_{i,j} &= -\sigma y_{i,j} - \beta x_{i,j} + D_2(y_{i+1,j} + y_{i-1,j} + y_{i,j+1} + y_{i,j-1} - 4y_{i,j}) + F \sin \omega t \\ &\equiv g(x_{i,j}, y_{i,j}), \qquad (18) \\ i, j &= 1, 2, \cdots, N. \end{aligned}$$

This two dimensional array has $N \times N$ cells arranged in a square lattice. In our numerical study we will again take $N = 100$.

In the following sections we present some of the interesting dynamical features exhibited by the above arrays of coupled MLC circuits such as active wave propagation and its failure, effect of weak coupling in the propagation, Turing patterns, effect of external periodic forcing on the Turing patterns and spatiotemporal chaotic dynamics. We have used *zero flux* boundary conditions for the study of propagation phenomenon and Turing patterns and *periodic* boundary conditions for the study of spatiotemporal chaos in our analysis.

5 Spatiotemporal patterns in autonomous CNNs: wave phenomena and Turing patterns

Transport processes in living tissues, chemical and physical systems have been often found to be associated with a special type of waves, namely, active waves. In the previous section we have seen a class of such active waves which arise in many reaction-diffusion systems. The important aspect in the reaction-diffusion CNNs is the wave propagation failure which occurs when the interconnections are weak, that is, for low values of coupling strength, a feature which *can not* be realized in the continuum limit as proved by Keener[17] in continuous homogeneous reaction-diffusion systems. Interestingly, experiments on biological systems shows that there exists a variety of situations where such failure in wave propagation do arise. We will identify such possibilities in the arrays of coupled MLC circuits.

5.1 Active wave propagation and its failure in one dimensional CNNs

To illustrate the wave propagation failure we consider the CNN model described by the array of coupld MLC circuits in one dimension, Eqs. (15). For this purpose we have numerically integrated Eqs. (15) using fourth order Runge-Kutta method with fixed step. In this analysis we fix the parameters at $\{\beta, \sigma, m_0, m_1, m_2, \epsilon, F\} = \{1.0, 1.0, -2.25, 1.5, .25, 0, 0\}$ so that the system admits

bistability which is a necessary condition to observe a wave front. Zero flux boundary conditions are used in the numerical computations, which in this context mean setting $x_0 = x_1$ and $x_{N+1} = x_N$ at each integration step; similar choice has been made for the variable y also. To start with, we will study in this section the autonomous case ($F = 0$) and extend our studies to the nonautonomous case ($F \neq 0$) in the next section.

The choice of the values of the parameters guarantees the existence of two stable equilibrium points $P_i^+ = \{\sigma(m_1 - m_0 - \epsilon)/(\beta + m_2\sigma),\ \beta(m_0 - m_1 - \epsilon)/(\beta + m_2\sigma)\}$ and $P_i^- = \{\sigma(m_1 - m_0 - \epsilon)/(\beta + m_1\sigma),\ \beta(m_0 - m_1 - \epsilon)/(\beta + m_1\sigma)\}$ for each cell, $i = 1, 2, \ldots, 100$. In the particular case corresponding to the above parametric choice, each cell in the array has three equilibrium points

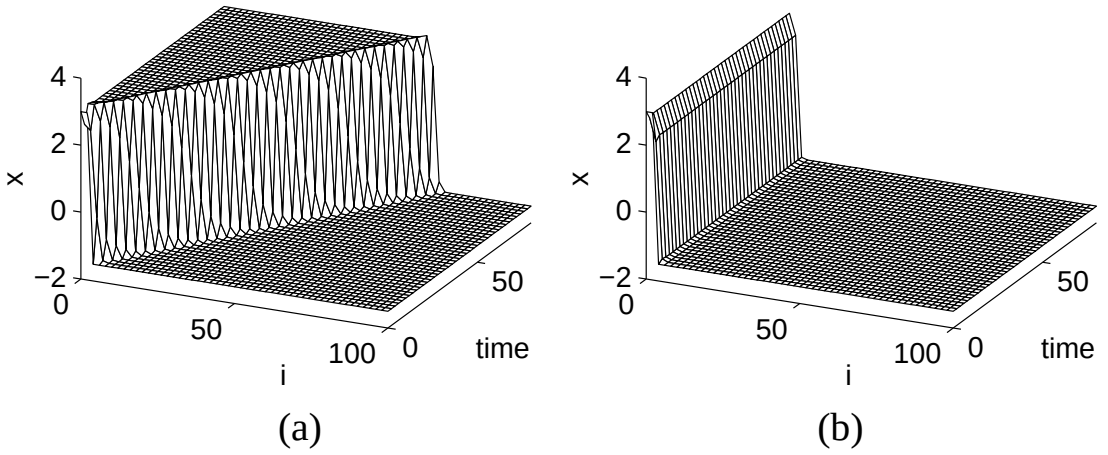

Figure 6: Space-time plot showing (a) propagation of wave fronts in one dimensional array (100 cells) of MLC circuits for $D = 2.0$ and (b) propagation failure for $D = 0.4$.

$P_i^+ = (3.0, -3.0)$, $P_i^- = (-1.5, 1.5)$ and $P_i^0 = (0, 0)$. Out of these three equilibrium points, P_i^+ and P_i^- are stable while P_i^0 is unstable. Due to the asymmetry in the function $h(x)$ for the present parametric choices, the basin of attraction of the point P_i^+ is much larger than that of P_i^- and it is harder to steer a trajectory back into the basin P_i^- once it is in the basin of P_i^+.

Now we choose an initial condition such that the first few cells in the array are excited to the P_i^+ state (having a large basin of attraction compared to that of P_i^-) and the rest are set to P_i^- state. In other words a wave front in the array is initiated by means of the two stable steady states. On actual numerical integration of Eqs.(15) with $N = 100$ and with the diffusion coefficient chosen at a higher value, $D = 2.0$, a motion of the wave front towards right (see Fig. 6(a)) is observed, that is a travelling wave front is found. After about 80 time units the wave front reaches the 100^{th} cell so that all the cells are now settled at the more stable state (P_i^+) as demonstrated in Fig. 6(a). When the value of D is decreased in steps and the analysis is repeated, the phenomenon of travelling wavefronts continues to be present.

However, below a critical value of the diffusion coefficient ($D = D_c$) a failure in the propagation has been observed, which in the present case turns out to be $D = D_c = 0.4$. This means that the initiated wavefront is unable to move as time progresses and Fig. 6(b) shows the propagation failure for $D = 0.4$.

5.2 Propagation failure mechanism: A case study

In the above, we have discussed the phenomenon of wavefront propagation and its failure in the one dimensional array of MLC circuits by numerically integrating eqs. (15) for $N = 100$ cells. In order to understand the mechanism behind wave propagation for large coupling strengths and its failure for low values of the intercell coupling, it is more advantageous to deal with fewer number

of cells such as $N = 3, 4, 5, 6$,etc. rather than $N = 100$ because of the diffuculties in handling large number of cells and equations analytically. For example one has to deal with the existence of 3^N steady states, which is quite large for $N = 100$, while it is manageble for $N = 3, 4$ or 5. With this fact in mind, we analyse analytically the case $N = 3$ and investigate the stability of the stationary states in order to understand the nature of bifurcations. A more detailed calculation for $N = 5$ is given elsewhere[39]. One can easily check that for $N = 3$ there are $3^3 = 27$ steady states. They may be obtained from the following set of defining equations:

$$\begin{aligned}
\dot{x}_1 &= y_1 - h(x_1) + D(x_2 - x_1), \\
\dot{x}_2 &= y_2 - h(x_2) + D(x_1 - 2x_2 + x_3), \\
\dot{x}_3 &= y_3 - h(x_3) + D(x_2 - x_3), \\
\dot{y}_j &= -\sigma y_j - \beta x_j, \quad j = 1, 2, 3,
\end{aligned} \tag{19}$$

where $h(x)$ is as given in Eq. (14) and the parameters are fixed at $\beta = 1$, $\sigma = 1$, $m_0 = -2.25$, $m_1 = 1.5$, $m_2 = 0.25$ and $\epsilon = 0$.

5.2.1 Linear stability analysis

Now let us consider the wave propagation. It is well known that the propagation failure is due to the existence of a large number of stationary states in the system[17]. Since we have considered the coupled system with three oscillators only there exists relatively few steady states. As we are looking for the wave front solution, it is sufficient to analyse the stability of only a subset of the possible 27 states. This can be done by considering six possible steady states in the following way: (i) the ultimate steady states, namely, X_P^+, X_P^0 and X_P^-, which exist even in the absence of coupling and (ii) the next three steady states which form wave front solutions, namely, X_S^+, X_S^0 and X_S^-. The steady states X_S^+, X_S^0 and X_S^- can be found by assuming the first cell in the P^+ state and the last cell in the P^- state and allowing the middle cell to be in one of the three available states, P^+, P^0, P^-. For example, X_S^+ state is obtained by considering the middle cell in the P^+ state. In a similar fashion the rest of the states, X_S^0 and X_S^-, are obtained. All the six steady states can be explicitly given as below:

$$\begin{aligned}
X_P^+ &= \{3, 3, 3, -3, -3, -3\} \\
X_P^0 &= \{0, 0, 0, 0, 0, 0\} \\
X_P^- &= \{-1.5, -1.5, -1.5, 1.5, 1.5, 1.5\}
\end{aligned} \tag{20}$$

$$\begin{aligned}
X_S^+ &= \{x_{1s}^+, x_{2s}^+, x_{3s}^+, y_{1s}^+, y_{2s}^+, y_{3s}^+\} \\
X_S^0 &= \{x_{1s}^0, x_{2s}^0, x_{3s}^0, y_{1s}^0, y_{2s}^0, y_{3s}^0\} \\
X_S^- &= \{x_{1s}^-, x_{2s}^-, x_{3s}^-, y_{1s}^-, y_{2s}^-, y_{3s}^-\}
\end{aligned} \tag{21}$$

where

$$\begin{aligned}
x_{1s}^+ &= \frac{3(8D^2 + 70D + 25)}{32D^2 + 70D + 25}, \qquad x_{2s}^+ = \frac{3(8D^2 + 40D + 25)}{32D^2 + 70D + 25}, \\
x_{3s}^+ &= \frac{1.5(16D^2 - 40D - 25)}{32D^2 + 70D + 25}, \quad y_{is}^+ = -x_{is}^+, \quad i = 1, 2, 3, \\
x_{1s}^0 &= \frac{15(6D - 5)}{16D^2 + 10D - 25}, \qquad x_{2s}^0 = \frac{30D}{16D^2 + 10D - 25}, \\
x_{3s}^0 &= \frac{-7.5(4D - 5)}{16D^2 + 10D - 25}, \qquad y_{is}^0 = -x_{is}^0, \quad i = 1, 2, 3, \\
x_{1s}^- &= -\frac{0.6(4D^2 - 20D - 25)}{4D^2 + 10D + 5}, \quad x_{2s}^- = -\frac{0.3(8D^2 + 20D + 25)}{4D^2 + 10D + 5}, \\
x_{3s}^- &= -\frac{0.3(8D^2 + 50D + 25)}{4D^2 + 10D + 5}, \quad y_{is}^- = -x_{is}^-, \quad i = 1, 2, 3.
\end{aligned} \tag{22}$$

The stability of the above steady states can be found by linearising (19) about them, which leads to the following Jacobian matrix:

$$J = \begin{pmatrix} -D - \frac{\partial h}{\partial x_1} & D & 0 & 1 & 0 & 0 \\ D & -2D - \frac{\partial h}{\partial x_2} & D & 0 & 1 & 0 \\ 0 & D & -D - \frac{\partial h}{\partial x_3} & 0 & 0 & 1 \\ -1 & 0 & 0 & -1 & 0 & 0 \\ 0 & -1 & 0 & 0 & -1 & 0 \\ 0 & 0 & -1 & 0 & 0 & -1 \end{pmatrix}, \tag{23}$$

where the derivatives, $\frac{\partial h}{\partial x_1}$, $\frac{\partial h}{\partial x_2}$ and $\frac{\partial h}{\partial x_3}$ are evaluated at the steady states. The stability is guaranteed if all the eigenvalues of the Jacobian matrix (23) have negative real parts. One can easily find that the states X_P^+ and X_P^- are asymptotically stable and X_P^0 is unstable irrespective of the values of D. However, on a careful analysis on the eigenvalues of the Jacobian for the nontrivial steady states, one can find the following: the state X_S^+ is asymptotically stable for $D < 0.3917$ and X_S^- is asymptotically stable for $D < 0.5178$ while X_S^0 is unstable irrespective of the D values. Thus any initial condition in the neighbourhood of X_s^+ (X_S^-) will eventually return to X_S^+ (X_S^-) as long as $0 < D \leq 0.3916$ ($0 < D \leq 0.5177$). Further, an arbitrary initial condition will evolve to a steady state which lies in the neighbourhood of it. As a consequence, the system with a low value of the diffusion coefficient for an initial condition lying in the basin of attraction of X_S^+ or X_S^- will transit to the corresponding stable states X_S^+ or X_S^- respectively and so a failure of propagation occurs. However, for $D > D_c$, the relevant steady loses stability and consequently the systems transits to a suitable final steady state which is stable and this turns out to be X_P^+. As a result wavefront propagation occurs. Further it may so happen that a given initial condition may or may not lie in the basin of attraction of a particular steady state X_S^+ or X_S^-, for a specific value of D in which case propagation does occur. Taking this fact also into account, one can prove that for the chosen initial conditions described in the numerical analysis above one finally obtains $D = D_c = 0.4$. Thus the wave front propagation occurs when the steay states lose their stability via a subcritical bifurcation.

The above analysis has been extended to the cases $N = 4, 5$ or 6 and one indeed draws the same conclusion as above. Thus we can explain the propagation failure at a critical value $D = D_c$ as due to the existence of stationary states combined with their basin of attraction.

5.3 Effect of weak coupling

In the above, the investigation has been made by considering the system as an ideal one (as far as the circuit parameters are concerned). But from a practical point of view, there are defects in the coupling parameters which may result in a weak coupling at any of the cell in the array. In the following we study the effect of such weak coupling on the propagation of wave front.

Let us consider a weak coupling at the k^{th} cell. By this we mean that the k^{th} cell in the array is coupled to its nearest neighbour $(k+1)^{\text{th}}$ and $(k-1)^{\text{th}}$ cells by resistors with slightly higher values than that of the others. We have studied the effect of this defect on the propagation of wave fronts. Numerical simulations have been carried out by considering an one dimensional array with 100 cells, where the initial conditions are chosen as in the case of propagation phenomenon in regular one dimensional arrays (see Sec. 5.1). From the numerical simulation results, we find that there is an abrupt stop in the propagation when the wave front reaches the weakly coupled cell. This happens when the coupling coefficient on either side of the k^{th} cell in the array has a value even above the critical value ($D = 0.4$) for propagation failure discussed in Sec. 5.1. Fig. 7 shows a blocking in the propagation of the wave front when the coupling coefficients on either side of the k^{th} cell ($k = 25$), which we call as D_k, is set to 0.47173 with the rest of the coupling coefficients set to 1 ($D = 1$). We observe that the actual blocking occurs when the wave front reaches the k^{th} cell. We can say that this is a kind of failure in the propagation because the wavefront will never reach the last cell (that is the 100^{th} cell in the array) by means of blocking. Here the existence

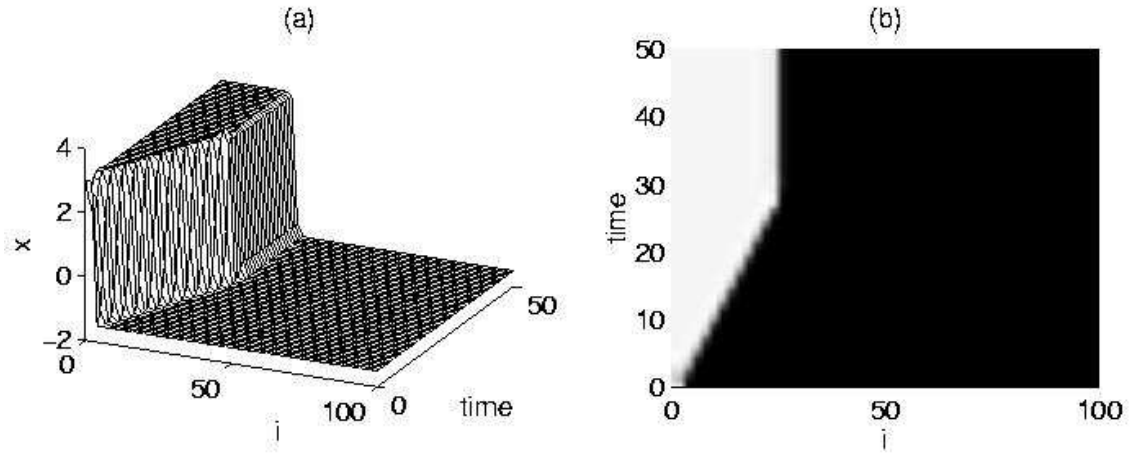

Figure 7: Figure showing the effect of weak coupling at the 25^{th} cell in the one dimensional array (Eq. (16)). (a) three dimensional space-time plot and (b) density plot.

of stable steady states at the k^{th} cell due to the weak coupling is responsible for the blocking of wave front. A stability analysis in the present case can be done as in the defect free case and one can conclude that the subcritical bifurcation is the cause of blocking.

5.4 Turing patterns

Another interesting dynamical phenomenon in the coupled arrays is the formation of Turing patterns. These patterns are observed in many reaction diffusion systems when a homogeneous steady state which is stable due to small spatial perturbations in the absence of diffusion becomes unstable in the presence of diffusion[11]. To be specific, the Turing patterns can be observed in a two variable reaction-diffusion system when one of the variables diffuses faster than the other and undergo Turing bifurcation, that is, diffusion driven instability[8, 11].

Treating the coupled array of MLC circuits as a discrete version of a reaction-diffusion system, one can as well observe the Turing patterns in this model also. For this purpose, one has to study the linear stability of system (3) near the steady state. In continuous systems, the linear stability analysis is necessary to arrive at the conditions for diffusion driven instability. A detailed derivation of the general conditions for the diffusion driven instability can be found in Murray[8]. For discrete cases one can follow the same derivation as in the case of continuous systems by considering solutions of the form $\exp i(kj - \lambda t)$[8, 40]. Here k and λ are considered to be independent of the position j ($j = 1, 2, \cdots, N$). For Eq. (3), the criteria for the diffusion driven instability can be derived by finding the conditions for which the steady states in the absence of diffusive coupling are linearly stable and become unstable when the coupling is present. One can easily show the eigenvalues that guarantee the linear stability in the absence of coupling are the roots of the characteristic equation

$$\lambda^2 - (f_x + g_y)\lambda + f_x g_y - f_y g_x = 0, \tag{24}$$

where f_x, f_y, g_x and g_y are the partial derivatives of f and g in Eq. (3) without coupling coefficients ($D_1 = D_2 = 0$) and evaluated at the steady state. It can be further seen easily that the steady state is stable in the absence of coupling if and only if the roots of (4) (λ_1 and λ_2) have negative real parts.

Apart from the above condition, in order to satisfy the instability in the presence of coupling (Turing instability), atleast one of the roots of the characteristic equation,

$$\lambda_s^2 - [k^2(D_1 + D_2) - (f_x + g_y)]\lambda_s + m(k^2) = 0, \tag{25}$$

with

$$m(k^2) = D_1 D_2 k^4 - (D_2 f_x + D_1 g_y)k^2 + f_x g_y - f_y g_x,$$

should have positive real part.

A straightforward calculation shows that the following conditions should be satisfied for the general reaction-diffusion system of the form given by Eq. (17):

$$\begin{aligned} f_x + g_y &< 0, \\ f_x g_y - f_y g_x &> 0, \\ f_x D_2 - g_y D_1 &> 0, \\ (f_x D_2 - g_y D_1)^2 - 4 D_1 D_2 (f_x D_2 - g_y D_1) &> 0. \end{aligned} \tag{26}$$

The critical wave number for the discrete system (3) can be obtained as

$$\cos(k_c) = 1 - \frac{f_x D_2 - g_y D_1}{4 D_1 D_2}. \tag{27}$$

Combining Eqs. (26)-(27), one obtains[39] the condition for the Turing instability such that

$$\frac{f_x D_2 - g_y D_1}{8 D_1 D_2} \leq 1. \tag{28}$$

We have applied these conditions to the coupled oscillator system of the present study. For this purpose, we have fixed the parameters for the two-dimensional model (3) as $\{\beta, \sigma, \epsilon, m_0, m_1, m_2\} = \{0.8,\ 0.92, 0.1, -0.5, 0.5, 0.5\}$ and verified that this choice satisfies the conditions (26) to (28). The numerical simulations have been carried out using an array of size 100×100 and random initial conditions near the steady states have been chosen for the x and y variables. Figs. 8(a)-8(d) show how the diffusion driven instability leads to stable hexagonal pattern (Fig. 8(d)) after passing through intermediate stages (Figs. 8(a)-8(c)). Further, the spontaneously formed patterns are fairly uniform hexagonal patterns having a penta-hepta defect pair. These defects are inherent and very stable.

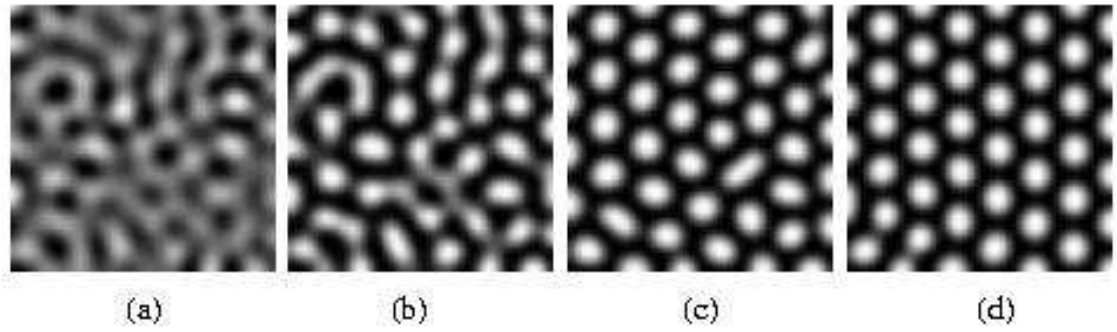

Figure 8: The spontaneous formation of Turing patterns in an array of 100×100 oscillators for the parameters $\beta = 0.8$, $\sigma = 1$, $m_0 = -0.5$, $m_1 = 0.5$, $m_2 = 0.5$, $\epsilon = 0.1$, $F = 0.0$, $\omega = 0.75$, $D_1 = 1$ and $D_2 = 10$ in Eq. (3) at various time units (a) $T = 50$, (b) $T = 100$, (c) $T = 500$ and (d) $T = 2000$ (e) the same figure (d) in the Fourier space.

6 Spatiotemporal patterns in the presence of periodic external force

The effect of external fields on a variety of dynamical systems has been studied for a long time as driven systems are very common from a practical point of view. These systems can be either spatially modulated or temporally modulated. For example, in a large number of dynamical

systems including the Duffing oscillator, van der Pol oscillator and the presently studied MLC circuits, temporal forcing leads to a variety of complex dynamical phenomena including bifurcations and chaos. In particular, it has been shown that the resonant coupling between the forcing and the oscillatory modes may lead to several complex dynamical patterns including quasiperiodicity, intermittency and chaos[38, 41, 42]. Also the studies on the effect of external fields in spatially extended systems have been receiving considerable interest in recent times[3, 43, 44]. Particularly, with the recent advances in identifying localized and oscillating structures and other spatiotemporal patterns in driven nonlinear dissipative systems such as granular media, driven Ginzburg-Landau equations and so on, it is of special interest to study the effects of forcing on arrays of coupled systems such as (3). Motivated by the above, we investigate the effect of external forcing on the propagation of wave front and formation of Turing patterns in the coupled MLC circuits in one and two dimensions.

6.1 Effect of external forcing on the propagation of wave fronts

In this subsection we study the effect of external forcing on the propagation of wave fronts. For this purpose we consider an one dimensional array of coupled MLC circuits with initial and boundary conditions as discussed in Sec. 5.1. Now we perform the numerical integration by the inclusion of external periodic force of frequency $\omega = 0.75$ in each cell of the array (see Eq. (1)). By varying the strength, F, of the external force we study the behaviour of the propagating wave front in comparison with the force free case ($F = 0$) as discussed in Sec. 5.1. We find that in the propagation region ($D > D_c$), the effect of forcing is just to introduce temporal oscillations and the propagation continues without any disturbance (see Fig. 9(a)) as in the case $F = 0$ (Fig. 6(a)). Of course this can be expected as the external force is periodic in time. However, interesting things happen in the propagation failure region discussed in Sec. 5.1. In this region, beyond a certain critical strength of the external forcing, the wavefront tries to move a little distance and then stops, leading to a partial propagation. Fig. 9(b) shows such a partial propagation observed for $F = 0.6$ and $D = 0.22$ (This may be compared with Fig. 6(b)). The phenomenon can be explained by considering the propagation failure mechanism discussed in Sec. 5.2 in which one may look for a spatially stationary and temporally oscillating wavefront. The initial wavefront tries to settle in the nearby stationary state. However, the system will take a little time and space to settle due the effect of forcing combined with the transient behaviour of the system. Thus the inclusion of external forcing in the propagation failure region can induce the wavefront to achieve a partial propagation.

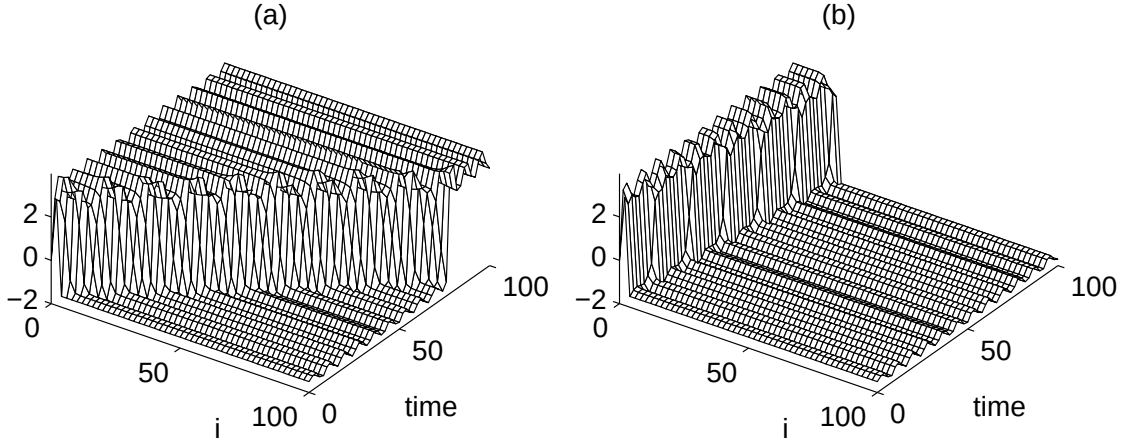

Figure 9: Propagation phenomenon in the presence of forcing: (a) Propagation of wavefront for $D = 2.0$ and $F = 0.6$ and (b) The partial propagation observed for $D = 0.22$ and $F = 0.6$.

6.2 Transition from hexagons to rhombs

It is well known that the defects are inherent in very many natural pattern forming systems. In most of the pattern forming systems, the observed patterns are not ideal. For example, the patterns are not of perfect rolls or hexagons or rhombs. A commonly observed defect in such systems is the so called penta-hepta defect (PHD) pair which is the bound state of two dislocations[45]. Experiments on spatially extended systems often show the occurrence of PHD in spontaneously developed hexagonal patterns[46] In the present case also, the existence of PHD pair can be clearly seen from Fig. 8(d). In such a situation, it is important to study the effect of external periodic force in the coupled arrays of MLC circuits.

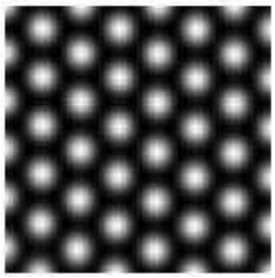

Figure 10: Figure showing the perfect organization of rhombic array in the presence of external periodic force with $F = 0.25$.

Now we include a periodic force with frequency ω and amplitude F in each cell of the array and we numerically integrate Eqs.(17) using fourth order Runge-Kutta method with zero flux at boundaries. By fixing the frequency of the the external periodic force as $\omega = 0.75$ and varying the amplitude (F) we analyse the pattern which emerges spontaneously. Interestingly for $F = 0.25$, the defects (PHD pair) which are present in the absence of external force (Fig. 8(d)), gets removed resulting in the transition to a regular rhombic array. Fig. 10 shows the gray scale plot of the pattern observed for $F = 0.25$. Thus, from the above we infer that the inclusion of external periodic force can cause a transition from hexagonal pattern to rhombic structures.

6.3 Transition from hexagons to rolls

In addition to the transition from hexagons to rhombs by the influence of external periodic force, there are also other possible effects due to it. To realize them, we consider a different set of parametric choice $\{\beta, \sigma, m_0, m_1, m_2\} = \{0.734722, 0.734722, -0.874, -0.4715, -0.4715\}$ with $\epsilon = 0.15$, $D_1 = 1.0$ and $D_2 = 5.0$. For this choice the system shows hexagonal patterns with defects including domains of small roll structures (Fig. 11(a)).

Now when the external periodic force is included a transition in the pattern from hexagonal structure to rolls starts appearing. By fixing the frequency of the external periodic force again at $\omega = 0.75$, we observed the actual transition from hexagons to rolls as we increase the forcing amplitude (F). Figs. 11(b)-11(d) show the gray scale plots for $F = 0.15$, 0.35 and 0.45, respectively. Obviously the transition is due to the existence of small roll structures in the pattern for $F = 0$ which nucleates the formation of rolls in the presence of forcing.

6.4 Breathing oscillations

In the above, we have shown that the inclusion of the external periodic force can make a transition from one stationary pattern to another stationary pattern like the transition from hexagons to rolls. Besides these, are there any time varying patterns? As mentioned above, patterns such as localized and breathing oscillations have considerable physical interest. In this regard, we considered the parameters $\{\beta, \sigma, \epsilon, m_0, m_1, m_2\} = \{0.734722, 0.734722, 0.10, -0.874, -0.4715, -0.4715\}$ with $D_1 = 2.0$ and $D_2 = 5.0$ such that a regular hexagonal pattern is observed in the

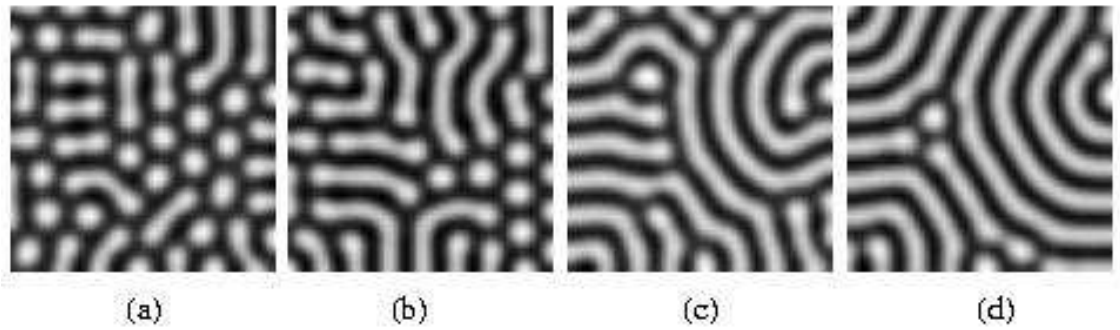

Figure 11: Figure showing the transition from hexagons to rolls for $\{\beta,\ \sigma,\ \epsilon,\ m_0,\ m_1,\ m_2\} = \{0.734722,\ 0.734722,\ 0.15,\ -0.874,\ -0.4715,\ -0.4715\}$ with $D_1 = 1$ and $D_2 = 5$. (a) $F = 0$, (b) $F = 0.15$, (c) $F = 0.35$ and (d) $F = 0.45$.

absence of external periodic force. From numerical simulations, we observed that a space-time periodic oscillatory pattern (breathing motion) sets in for a range of low values of F. Fig. 12 shows the typical snapshots of the oscillating pattern at various instants for the specific choice $F = 0.05$. We have integrated over 10000 time units and the figure corresponds to the region $T = 4000 - 4014$. Typically we find that the breathing pattern repeats itself approximately after a period $T = 15.0$ in the range of our integration. One may conclude that the emergence of such breathing oscillations is due to the competition between the Turing and Hopf modes in the presence of external periodic force.

7 Spatiotemporal chaos

Next we move on to a study of the spatiotemporal chaotic dynamics of the array of coupled MLC circuits when individual cells are driven by external periodic force. The motivation is that over a large domain of (F, ω) values the individual MLC circuits typically exhibit various bifurcations and transition to chaotic motion. So one would like to know how the coupled array behaves collectively in such a situation, for fixed values of the parameters. For this purpose, we set the parameters at $\{\beta, \sigma, \epsilon, m_0, m_1,\ m_2, \omega\} = \{1.0, 1.015, 0, -1.02, -0.55, -0.55, 0.75\}$. The uncoupled systems exhibit period doubling bifurcations and chaotic dynamics in the presence of external force. In our numerical simulations, we have mainly considered the one dimensional array specified by Eq. (1) and assumed periodic boundary conditions.

7.1 Spatiotemporal regular and chaotic motion

Numerical simulations were performed by considering 50 cells and random initial conditions using fourth order Runge-Kutta method for six choices of F values. The coupling coefficient in Eq. (15) was chosen as $D = 1.0$. Out of these, the first three lead to period-T, period-$2T$, period-$4T$ oscillations, respectively and the remaining choices correspond to chaotic dynamics of the single MLC circuit. Figs. 13(a)-13(g) show the space-time plots for $F = 0.05$, $F = 0.08$, $F = 0.09$, $F = 0.12$, $F = 0.13$ and $F = 0.15$, respectively. From the Figs. 13(a)-13(c), it can be observed that for $F = 0.05$, 0.08 and 0.09 the MLC array also exhibits regular periodic behaviour with periods T, $2T$ and $4T$ respectively in time alone as in the case of the single MLC circuit. However, for $F = 0.12$ and 0.13(Figs. 13(d) and 13(e)) one obtains *space-time periodic* oscillations eventhough each of the individual uncoupled MLC circuits for the same parameters exhibits chaotic dynamics. We may say that a kind of controlling of chaos occurs due to the coupling, though the coupling strength is large here. From the above analysis it can be seen that the macroscopic system shows regular behaviour in spite of the fact that the microscopic subsystems oscillate chaotically.

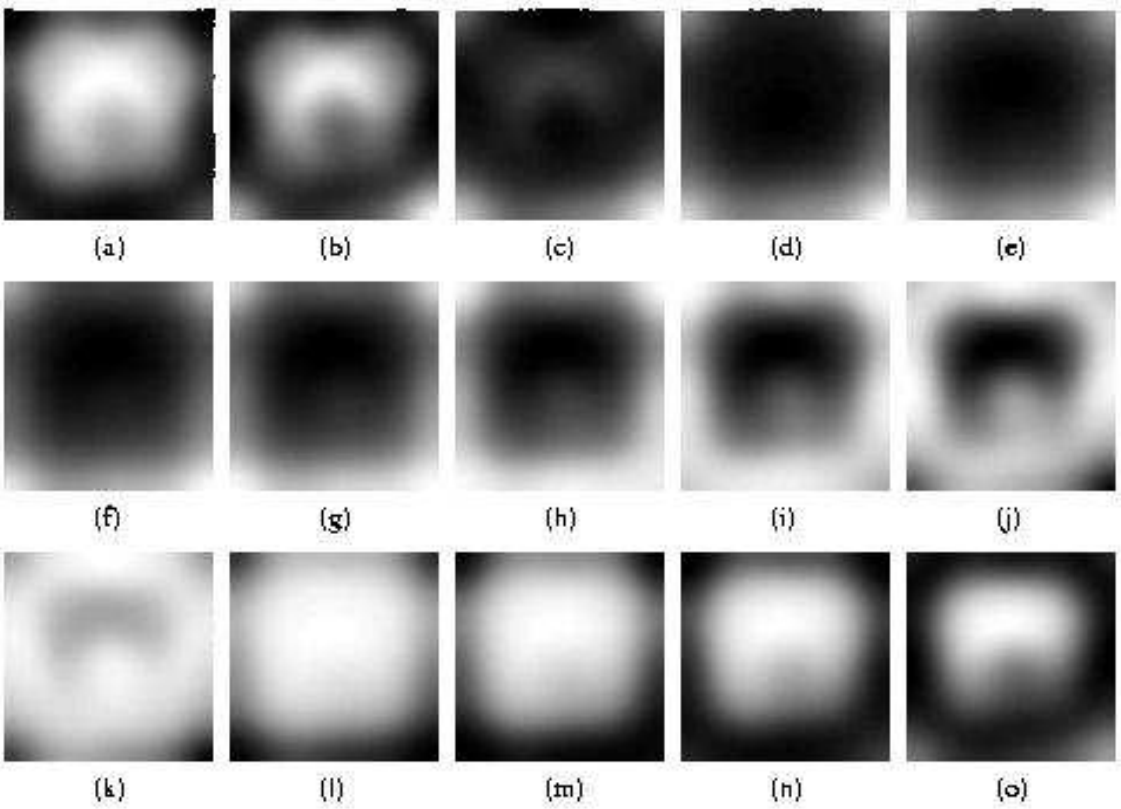

Figure 12: Snapshots showing breathing oscillations for $F = 0.05$ and $\{\beta, \sigma, \epsilon, m_0, m_1, m_2\} = \{0.734722, 0.734722, 0.15, -0.874, -0.4715, -0.4715\}$ with $D_1 = 2$ and $D_2 = 5$ for various time units starting from $T = 4001$.

Finally for $F = 0.15$ the coupled system shows spatiotemporal chaotic dynamics (Fig. 13(f)) and this was confirmed by calculating the Lyapunov exponents using the algorithm given by Wolf *et al*[50]. For example, we calculated the Lyapunov exponents for $N = 50$ coupled oscillators and we find the largest three exponents have the values $\lambda_{\max} = \lambda_0 = 0.1001$, $\lambda_1 = 0.0776$, $\lambda_2 = 0.0092$ and the rest are negative (see next subsection for further analysis).

7.2 Size instability, chaos synchronization and suppression of STC

Since the above study of spatiotemporal chaos involves a large number of coupled chaotic oscillators, it is of great interest to analyse the size dependence of the dynamics of these systems. To start with, we consider the case of 10 coupled oscillators with periodic boundary conditions and numerically solve the system with the other parameters chosen as in Sec. 7.1. The value of F is chosen in the range $(0.12, 0.15)$. We find that this set up shows a different behaviour as compared to the 50 cells case. Actually the system gets synchronized to a chaotic orbit rather than showing periodic behaviour or spatiotemporal chaos as in the case of 50 cells described above.

To start with we analyse the dynamics for $F = 0.12$ by slowly increasing the system size from $N = 10$. It has been found that the coupled system (15) shows synchronized motion for $N \leq 42$. This was confirmed by calculating the Lyapunov spectrum which shows only one positive exponent with the rest being negative. For example, for $N = 42$, $\lambda_{\max} = 0.1162$, with the rest of the exponents being negative. The existence of only one positive exponent is a necessary condition to have chaos synchronization[51]. Fig. 14(a) shows the dynamics of the 5^{th} cell in the array. The system shows entirely different behaviour when we increase the system size to $N = 43$. As

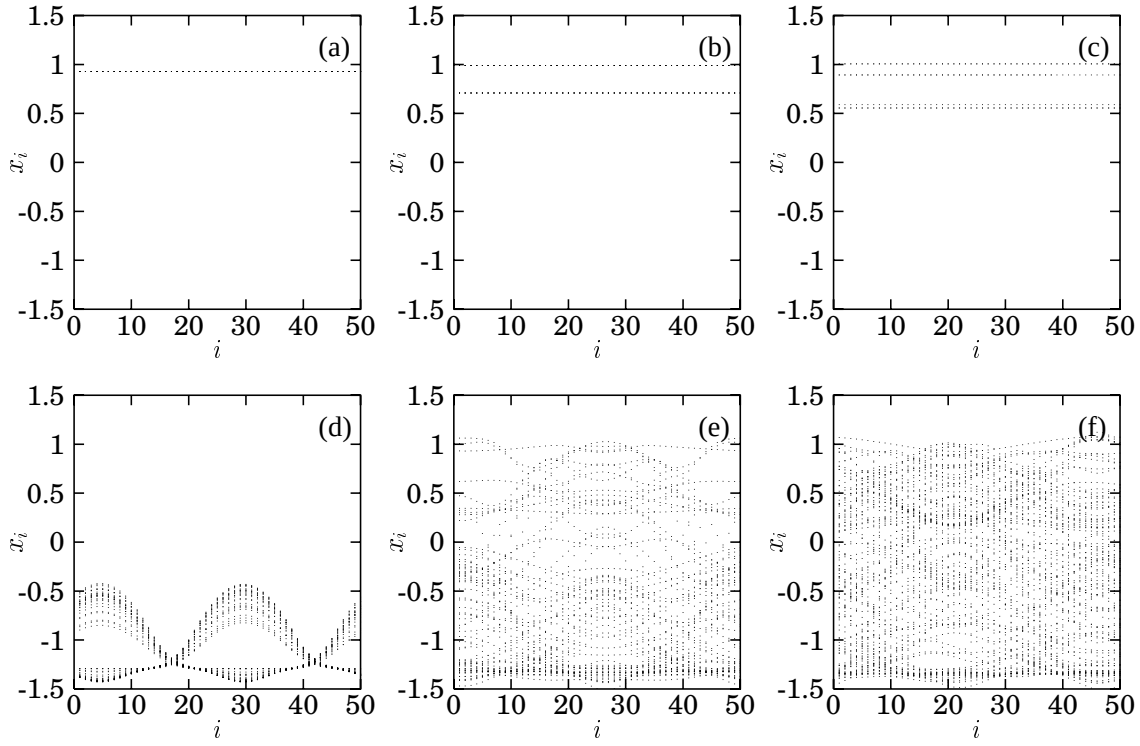

Figure 13: Space-amplitude plot showing the spatiotemporal periodic and chaotic oscillations in 50 coupled MLC circuits for various values of external periodic forcing strength: (a) $F = 0.05$, (b) $F = 0.08$, (c) $F = 0.091$, (d) $F = 0.12$, (e) $F = 0.13$ and (f) $F = 0.15$.

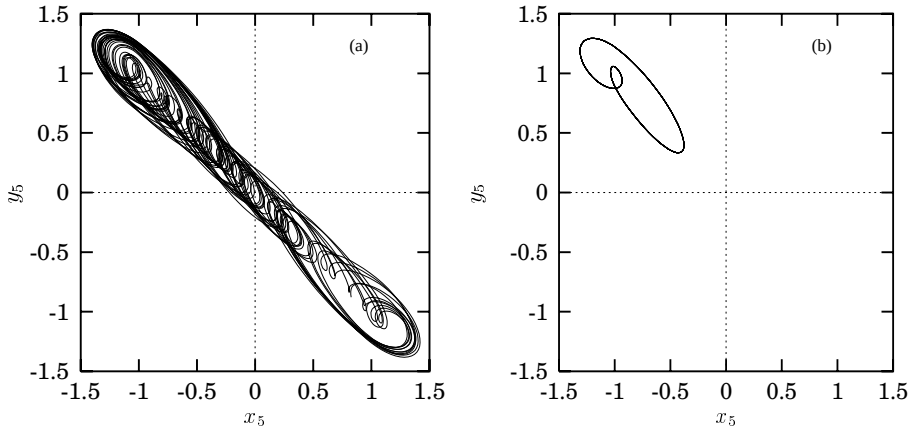

Figure 14: (a) The chaotic attractor at the 5^{th} cell for the synchronized state ($N = 42$) and (b) the periodic orbit in the 5^{th} cell for the controlled state ($N = 43$)

noted in the previous subsection, 7.1, there occurs a kind of suppression of spatiotemporal chaos. Fig. 14(b) shows the resultant periodic orbit in the 5^{th} cell of the array. The maximal Lyapunov exponent is found to be negative in this case ($\lambda_{\max} = -0.001474$). Similar phenomenon has been observed for $F = 0.13$ also.

Next we consider the case of $F = 0.15$ in which the coupled system in the previous subsection showed spatiotemporal chaos. From numerical simulations, we again observed a synchronized motion for $N \leq 31$ and the corresponding Lyapunov spectrum shows one positive exponent only with

all the other exponents being negative. But for $N > 31$, the coupled system shows spatiotemporal chaos. The Lyapunov spectrum in this case (for $N > 31$) possesses multiple positive exponents. For example, for $N = 43$, ($\lambda_{\max} = \lambda_0 = 0.0997$, $\lambda_1 = 0.0633$, $\lambda_2 = 0.0038$).

The above type of size instability behaviour has also been found in a coupled Rössler system as well which undergoes a short wavelength bifurcation[52]. In such cases, one can find the exact value of the size below which stable synchronous oscillations occur. However, we find that the coupled MLC circuits do not show short wavelength bifurcations. To arrive at a criteria for the size instability we computed the Lyapunov dimension. It has been noted that the fractal dimension per unit size, dimension density, is an appropriate quantity for the spatiotemporal chaotic systems[15, 16]. A detailed analysis on the size instability and chaos synchronization in coupled system (15) will be reported elsewhere.

8 Conclusions

In this lecture/article, we have tried to point out how reactive diffusive nonliear systems can give rise to a wide variety of spatiotemporal patterns ranging from trivial homogeneous states and travelling wavefronts to Turing patterns and spatiotemporal chaos. However even wider phenomena can be captured by discretized systems in the form of cellular neural/nonlinear networks. As typical examples we considered one and two dimensional arrays of coupled MLC circuits and showed a wavefront propagation failure can occur due to certain subcritical bifurcations. The onset of various interesting patterns including Turing patterns such as hexagons, rhombs, rolls and the effect of external forcing on them leading to breathing oscillations were demonstrated. Finally how transitions to spatiotemporal chaos and synchronization occurs and the role of system size in these transitions have been brought out.

What has been demonstrated here is only a miniscule of the various phenomena on a space-time scale which can occur in nonlinear reactive diffusive systems in general and CNNs in particular. Even these basic patterns can play a very useful role in developing synchronized communication systems, patterns recognition, image processing and so on. Much more work need to be done in order discern all basic patterns which can arise in CNNs and to understand their structure and stability. This can in turn will lead to a better understanding of nonlinear dynmaical systems in general.

Acknowledgements

The work of M.L. forms part of Department of Science & Technology sponsored Govt. of India research project. The work of P.M. has been supported by Council of Scientific & Industrial Research through a Senior Research Fellowship.

References

[1] R A Fisher Ann Euginics **7** (1937) 355

[2] M C Cross and P C Hohenberg Rev Mod Phys **63** (1993)

[3] D Walgraef *Spatio-temporal Pattern Formation* Springer-Verlag New York (1996) pp 127

[4] A Okubo *Diffusion and Ecological Problems: Mathematical Models* Springer-Verlag (1980)

[5] A Koch and H Meinhardt Rev Mod Phys **66** (1994) 1481

[6] A C Scott Rev Mod Phys **47** (1975) 487

[7] M Bushev *Synergetics Chaos, Order, Self-organization* World Scientific Singapore (1994)

[8] J D Murray *Mathematical Biology* Springer-Verlag NewYork (1989)

[9] A V Holden Phys World **11** (1998) 29

[10] T Amemiya et al Chaos **8** (1998) 872

[11] A M Turing Phil Trans Roy Soc London **B237** (1952) 37

[12] P B Umbanhowar F Melo and H L Swinney Nature **382** (1996) 793

[13] J Fineberg Nature **382** (1996) 763

[14] R J Deissler and H R Brand Phys Rev Lett **74** (1995) 4847

[15] D A Egolf and H S Greenside Nature **369** (1994) 124

[16] T Bohr E Bosch and W van de Water Nature **372** (1994) 48

[17] J P Keener SIAM J Appl Math **47** (1987) 556

[18] L O Chua *CNN: A Paradigm for Complexity* World Scientific Singapore (1998)

[19] L O Chua (Ed) Special issue on "Nonlinear waves, patterns and spatio-temporal chaos in dynamic arrays" IEEE Trans Circ Syst **42** (1995) 557

[20] Y Kuramoto *Chemical Oscillations, Wave and Turbulence* Springer-Verlag New York (1984)

[21] J L Marín and S Aubry Nonlinearity **9** (1996) 1501-1528

[22] S Watanabe S H Strogatz and van der Zant Phys Rev Lett **74** (1995) 379

[23] M Dolnik and M Marek J Phys Chem **92** (1988) 2452

[24] J P Laplante and T Erneux Physica A **188** (1992) 89

[25] M A Allesie F I M Bonke and T Y G Scopman Circ Res **33** (1973) 54

[26] M Feingold et al Phys Rev A **37** (1988) 4060

[27] A P Muñuzuri et al IEEE Trans Circ Syst **40** (1993) 872

[28] V Pérez-Muñuzuri et al Int J Bifur Chaos **3** (1993) 211

[29] T Sobrino et al Eur J Phys **14** (1993) 74

[30] V Pérez-Muñuzuri et al Int J Bifur Chaos **4** (1994) 1631

[31] V Pérez-Muñuzuri et al Physica D **82** (1995) 195

[32] L Kocarev and U Parlitz Phys Rev Lett **77** (1996) 2206

[33] O Lioubasheski H Arbell and J Fineberg Phys Rev Lett **76** (1996) 3959

[34] A Kudrolli M Wolpert and J P Gollub Phys Rev Lett **78** (1997) 1383

[35] P Bak K Chen Sci Am **264** (1991) 46

[36] K Murali M Lakshmanan and L O Chua IEEE Trans Circ Sys **I41** (1994) 462

[37] M Lakshmanan and K Murali Phil Trans R Soc Lond A **353** (1995) 33

[38] M Lakshmanan and K Murali *Chaos in Nonlinear Oscillators: Controlling and Synchronization* World Scientific Singapore (1996)

[39] P Muruganandam K Murali and M Lakshmanan Int J Bifur Chaos **9** (1999) 805

[40] A P Muñuzuri et al Int J Bifur Chaos **5** (1995) 17

[41] J Guckenheimer and P Holmes *Nonlinear Oscillations, Dynamical Systems and Bifurcation of Vector fields* Springer Verlag New York (1983)

[42] Hao Bai-Lin *Chaos* World Scientific Singapore (1984)

[43] D Walgraef Europhys Lett **7** (1988) 485

[44] L Pismen Phys Rev Lett **59** (1987) 2740

[45] L S Tsimring Physica D **89** (1996) 368

[46] J Pantaloni and P Cerisier in *Cellular Structures and Instabilities, Leccture Notes in Physics* **210** Eds J E Wesfreid and S Zaleski Springer-Verlag Berlin (1983)

[47] J J Perraud et al Phys Rev Lett **71** (1993) 1272

[48] K Murali M Lakshmanan and L O Chua Int J Bifur Chaos **4** (1994) 1511

[49] K Murali M Lakshmanan and L O Chua Int J Bifur Chaos **5** (1995) 6498

[50] A Wolf et al Physica D **16** (1985) 285

[51] L M Pecora and T L Carroll Phys Rev Lett **64** (1990) 821

[52] J F Heagy T L Carroll and L M Pecora Phys Rev Lett **74** (1994) 4185